# AFRL-ML-WP-TP-2006-405

# COMPARATIVE ANALYSIS OF THREE FRETTING FATIGUE FIXTURES (PREPRINT)

**Patrick J. Golden, Alisha L. Hutson, Bence B. Bartha, and Theodore Nicholas**


**FEBRUARY 2006**

**Approved for public release; distribution is unlimited.**

**STINFO FINAL REPORT**



**MATERIALS AND MANUFACTURING DIRECTORATE**
**AIR FORCE RESEARCH LABORATORY**
**AIR FORCE MATERIEL COMMAND**
**WRIGHT-PATTERSON AIR FORCE BASE, OH 45433-7750**

# NOTICE

Using Government drawings, specifications, or other data included in this document for any purpose other than Government procurement does not in any way obligate the U.S. Government. The fact that the Government formulated or supplied the drawings, specifications, or other data does not license the holder or any other person or corporation; or convey any rights or permission to manufacture, use, or sell any patented invention that may relate to them.

This report was cleared for public release by the Air Force Research Laboratory Wright Site (AFRL/WS) Public Affairs Office (PAO) and is releasable to the National Technical Information Service (NTIS). It will be available to the general public, including foreign nationals.

PAO Case Number: AFRL/WS 06-0296, 6 Feb 06.

THIS TECHNICAL REPORT IS APPROVED FOR PUBLICATION.

/s/

PATRICK J. GOLDEN
Metals Branch
Metals, Ceramics and NDE Division

/s/

ROLLIE DUTTON, Chief
Metals Branch
Metals, Ceramics and NDE Division

/s/

GERALD J. PETRAK, Asst Chief
Metals, Ceramics and NDE Division
Materials and Manufacturing Directorate

This report is published in the interest of scientific and technical information exchange and its publication does not constitute the Government's approval or disapproval of its ideas or findings.

# REPORT DOCUMENTATION PAGE

*Form Approved*
*OMB No. 0704-0188*



| 1. REPORT DATE *(DD-MM-YY)* | 2. REPORT TYPE | 3. DATES COVERED *(From - To)* |
|---|---|---|
| February 2006 | Journal Article Preprint | |

**4. TITLE AND SUBTITLE**
COMPARATIVE ANALYSIS OF THREE FRETTING FATIGUE FIXTURES (PREPRINT)

**5a. CONTRACT NUMBER**
In-house

**5b. GRANT NUMBER**

**5c. PROGRAM ELEMENT NUMBER**
62102F

**6. AUTHOR(S)**
Patrick J. Golden and Bence B. Bartha (AFRL/MLLMN)
Alisha L. Hutson (University of Dayton Research Institute)
Theodore Nicholas (AFIT/ENY)

**5d. PROJECT NUMBER**
4347

**5e. TASK NUMBER**
RG

**5f. WORK UNIT NUMBER**
M02R3000

**7. PERFORMING ORGANIZATION NAME(S) AND ADDRESS(ES)**

Metals Branch (AFRL/MLLMN)
Metals, Ceramics and NDE Division
Materials and Manufacturing Directorate
Air Force Research Laboratory, Air Force Materiel Command
Wright-Patterson AFB, OH 45433-7750

University of Dayton Research Institute
Dayton, OH 45469-0128

---

Air Force Institute of Technology (AFIT/ENY)
Wright-Patterson AFB, OH 45433-7765

**8. PERFORMING ORGANIZATION REPORT NUMBER**
AFRL-ML-WP-TP-2006-405

**9. SPONSORING/MONITORING AGENCY NAME(S) AND ADDRESS(ES)**
Materials and Manufacturing Directorate
Air Force Research Laboratory
Air Force Materiel Command
Wright-Patterson AFB, OH 45433-7750

**10. SPONSORING/MONITORING AGENCY ACRONYM(S)**
AFRL/MLLMN

**11. SPONSORING/MONITORING AGENCY REPORT NUMBER(S)**
AFRL-ML-WP-TP-2006-405

**12. DISTRIBUTION/AVAILABILITY STATEMENT**
Approved for public release; distribution is unlimited.

**13. SUPPLEMENTARY NOTES**
Report contains color.



**14. ABSTRACT**
Three fixtures for conducting laboratory fretting fatigue tests are described and their respective testing methods and the results of the analysis are compared. Each of these fixtures has been used to investigate the effects of various parameters of interest in fretting fatigue. These fixtures include a unique apparatus in which all load applied to the specimen is transferred to the fretting pads, an apparatus similar to many found in the literature where partial load transfer occurs across the pads, and a simplified dovetail fixture in which the clamping load, *P*, and the shear load, *Q*, are varied in phase. Select test conditions from prior experiments performed on identical material and resulting in similar lives ranging from 1 to 10 million cycles from these fixtures are identified. The various testing conditions were used to compute the unique stress field for each case. The resulting contact stresses were used to calculate crack initiation based criteria, and to calculate stress intensity factors. The three fixtures were shown to be able to accommodate a range of loads, fretting pad contours, and specimen geometries that produced a variety of stress fields. A crack-initiation-based criterion was shown to predict the failure lives of thinner specimens accurately. The stress intensity factor calculations showed the possibility of a crack arresting for a stress field that decays rapidly and the possibility of a local minimum for K as a function of depth. The fixtures are shown to be complementary in generating data for development of robust fretting fatigue models that use these criteria.

**15. SUBJECT TERMS** Fretting, Fatigue, Life Prediction, Ti-6Al-4V

| 16. SECURITY CLASSIFICATION OF: | | | 17. LIMITATION OF ABSTRACT: | 18. NUMBER OF PAGES | 19a. NAME OF RESPONSIBLE PERSON (Monitor) |
|---|---|---|---|---|---|
| a. REPORT | b. ABSTRACT | c. THIS PAGE | | | Patrick Golden |
| Unclassified | Unclassified | Unclassified | SAR | 32 | 19b. TELEPHONE NUMBER *(Include Area Code)* |

# Comparative Analysis of Three Fretting Fatigue Fixtures

Patrick J. Golden[1], Alisha L. Hutson[2], Bence B. Bartha[3], Theodore Nicholas[4]

**Abstract**

Three fixtures for conducting laboratory fretting fatigue tests are described and their respective testing methods and the results of the analysis are compared. Each of these fixtures has been used to investigate the effects of various parameters of interest in fretting fatigue. These fixtures include a unique apparatus in which all load applied to the specimen is transferred to the fretting pads, an apparatus similar to many found in the literature where partial load transfer occurs across the pads, and a simplified dovetail fixture in which the clamping load, $P$, and the shear load, $Q$, are varied in phase. Select test conditions from prior experiments performed on identical material and resulting in similar lives ranging from 1 to 10 million cycles from these fixtures are identified. The various testing conditions were used to compute the unique stress field for each case. The resulting contact stresses were used to calculate crack initiation based criteria, and to calculate stress intensity factors. The three fixtures were shown to be able to accommodate a range of loads, fretting pad contours, and specimen geometries that produced a variety of stress fields. A crack-initiation-based criterion was shown to predict the failure lives of thinner specimens accurately. The stress intensity factor calculations showed the possibility of a crack arresting for a stress field that decays rapidly and the possibility of a local

[1] Materials Research Engineer, Air Force Research Laboratory, AFRL/MLLMN, Wright-Patterson AFB, OH 45433-7817, USA, Phone: 937-255-5438, FAX: 937-656-4840, patrick.golden@wpafb.af.mil
[2] Research Engineer, University of Dayton Research Institute, Dayton, OH 45469-0128, USA, Phone: 937-255-2708, FAX: 937-255-1363,alisha.hutson@wpafb.af.mil
[3] Materials Research Engineer, Air Force Research Laboratory, AFRL/MLLMN, Wright-Patterson AFB, OH 45433-7817, USA, Phone: 937-255-9368, FAX: 937-656-4840, bence.bartha@wpafb.af.mil
[4] Visiting Research Professor, Air Force Institute of Technology, AFIT/ENY, Wright-Patterson AFB, OH 45433-7765, USA, Phone: 937-255-3636x4537, FAX: 937- , theodore.nicholas.ctr@afit.edu

This work has been submitted to Society for Experimental Mechanics, Inc. for publication in Experimental Mechanics.

minimum for K as a function of depth. The fixtures are shown to be complementary in generating data for development of robust fretting fatigue models that use these criteria.

## 1. Introduction

Fretting fatigue is a problem that can lead to component damage or failure in applications where two components are in contact and undergo small cyclic relative motion, as in a dovetail slot in an aircraft turbine engine. Part of the difficulty in developing a robust model for fretting fatigue lies in the many conditions under which fretting wear and fretting fatigue may appear. Experimental techniques have been developed to simulate service conditions that include applied stresses, materials, contact geometry, time dependent contact interactions and environmental factors [1]. However, considerable difficulty has been encountered in applying the results of these investigations to service components, or even to other test geometries due to the interdependence of many of the critical parameters, and the localized nature of the phenomena.

The results of various efforts to model and predict fretting fatigue lives or fatigue limit stresses range from application of knockdown factors to determination of parameters for fretting fatigue limit stresses to fracture mechanics based methods involving thresholds for long lives or crack growth rate calculations for shorter lives. Knockdown factors must be determined empirically, and are therefore, limited to specific contact and material conditions. The stress-based approach to fretting fatigue life prediction based on maximum stresses at the surface generally under-predicts fretting fatigue life and is also limited to given contact conditions [2]. Fracture mechanics methods have heretofore been unable to demonstrate the existence of threshold conditions under a variety of experimental conditions [3]. While each technique or combination thereof has its merits, none have been demonstrated to be solely applicable to

service components because of the complexity of the component geometry as well as the wide range of loading conditions to which the components are subjected.

Data for modeling efforts are normally generated using a single experimental apparatus in most laboratories. While the extension of modeling from one geometry to another is a worthwhile cause, the practicality of having well documented and complementary conditions often precludes such an undertaking. An assessment of the literature does not indicate that one can define a "best" apparatus for performing fretting fatigue experiments and generating the most useful and relevant data. The authors have the benefit of having three different fretting fatigue test fixtures in one laboratory on which experiments have been performed on identical material and in similar total life ranges. The purpose of this paper is to compare these three test systems using various contact geometries and a range of applied loading conditions involving the clamping load, $P$, the resultant or applied shear load, $Q$, the bulk stress, $\sigma_{bulk}$, and friction coefficient $\mu$. Finite element and numerical contact mechanics analyses are used to calculate the stress fields for the various experimental loading conditions. Fracture mechanics methodology and a stress-life approach are employed to assess the experimental results. The merits of these modeling methods on each fixture are discussed in terms of the range of viable conditions and the unique features offered by each.

## 2. Experimental Background

### *2.1 Experimental Fretting Fixtures*

Three experimental fixtures used in the authors' laboratory were compared in this work. Each fixture was selected because of the unique features offered to allow investigation of different regimes in fretting fatigue, and availability of data from prior investigations. The first system, called "fixture A", is used to test relatively thin flat specimens against flat pads with

blending radii at the edges of contact (see Fig. 1) [4]. The entire load applied to the specimen is transferred to the fixture through the fretting pads. Thus, the portion of the specimen beyond the contact area is not subjected to the bulk cyclic load. Gross slip is eliminated throughout each test because the ratio of the normal load to the shear load is higher than the friction coefficient ($Q/P>\mu$), thus minimizing the fretting wear component of damage that tends to obscure small cracks. The shear force, $Q$, is simply equal to half the remotely applied bulk stress, $\sigma_{bulk}$, times the cross sectional area as in Eq. 1. In this fixture, $Q$ must be kept relatively small compared to the clamping force, $P$, so that the specimen does not slip out of the fretting pads. Additionally, values of $\sigma_{bulk}$ need to be high enough to represent conditions that occur in components. This drives the design of a thin specimen resulting in relatively high $\sigma_{bulk}$ and low $Q$.

$$Q = \frac{1}{2}\sigma_{bulk} A \qquad (1)$$

An additional capability of this fixture is that each test consists of two fretting tests loaded under nominally equal conditions. For each failure this results in a second test that has been loaded to "100% of life", but has not yet failed. To take advantage of the test data locked into the unfailed end of the fretting fatigue sample, a double-dogbone specimen has been developed and used in some prior experiments. These specimens were devised so that the fretting condition could be removed prior to fracture, and the resulting damage zone tested under uniaxial fatigue conditions to evaluate the effect of the damage on material fatigue strength [5]. Through fractography, any existing fretting cracks can then be identified and measure.

The second system, called "fixture B", uses a flat dogbone specimen contacted on both sides with cylindrical or short flat pads with blending radii at the edges of contact, as shown in Fig. 2 [6]. This fixture is typical of many reported in the literature [7]. Unlike fixture A, it produces partial transfer of the axial bulk load through the fretting pads due to friction, to a

nominally rigid fixture that controls the applied clamping load and pad alignment. The amount of load transfer from the specimen to the pads is controlled by the ratio of the specimen compliance and the fixture compliance. For a lower normal load relative to the shear load where the $Q/P$ ratio is closer to $\mu$, gross slip may occur during the run-in process until surface interactions increase the local coefficient of friction, $\mu$, to a steady state value, after which partial slip conditions prevail. Both cylindrical and rounded-flat pads were tested on this fixture. These pads have also been used in studies to determine the fatigue behavior of fretting initiated cracks using "C-Specimen" design [8]. Since the fretting pads have the same contact loading history as the specimens, less the bulk stress, they will also nucleate fretting cracks. The size and behavior of these fretting cracks have been studied.

The third system is a simplified dovetail fixture (Fig. 3), called "fixture C", in which the shear and clamping loads are the reactive forces to the applied loading and, therefore are both cyclic and in-phase with the applied load. The compliance of the specimen and fixture determine the normal, $P$, and shear, $Q$, load paths during the partial slip. The contact loads are determined indirectly through the use of strain gages on the fixture. $P$ and $Q$ are calculated using Finite Element Analysis (FEA) combined with the strain gage results as described in Golden and Nicholas [9] and based on prior work by Conner and Nicholas [10]. Flank angles of 35°, 45°, or 55° are incorporated in three variations of this fixture. Similar to the Fixture B setup, cylindrical or short flat pads with blending radii may be used in the experiments. Gross slip may occur during the run-in portion of the test for the reasons described for fixture B. Also, as in fixture B, a miniature "C-specimen" has been developed for fixture C. This miniature C-specimen can be machined from the fretting pads of fixture C and tested in precisely the same manner as described in Golden et al. [8], just on a smaller scale. Additionally, the miniature C-specimen

can be adapted to the dovetail specimen. It can be machined out of an unfailed side of the specimen or from both sides of an interrupted or runout specimen. The trailing edge of contact where cracks nucleate is located in the center of the "C". Again, use of the double dogbone, C-specimen, and mini-C-specimen are methods being used in the AFRL for gaining additional fretting crack data from each of the three experimental fixtures.

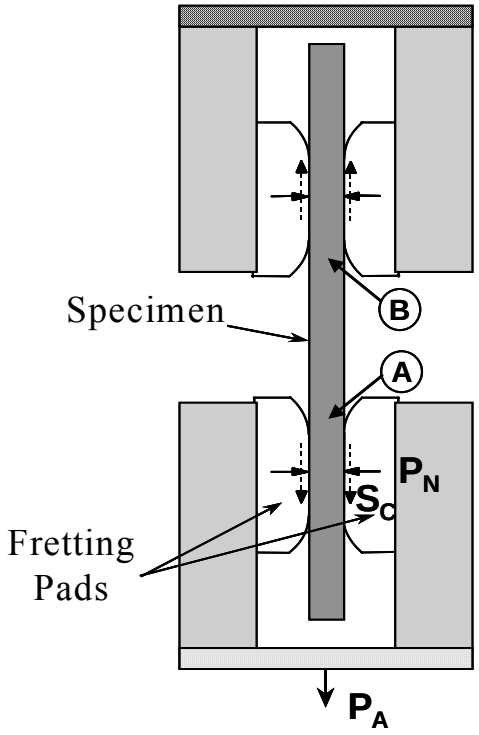


Fig. 1: Schematic of the full load transfer fixture, "A".

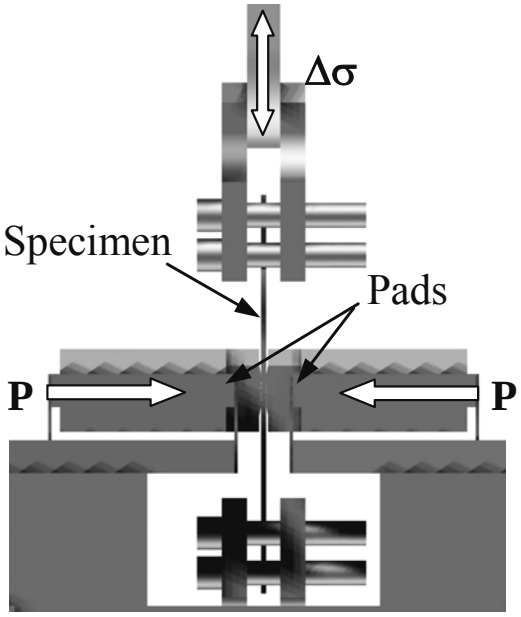


Fig. 2: Schematic of the partial load transfer fixture, “B”.

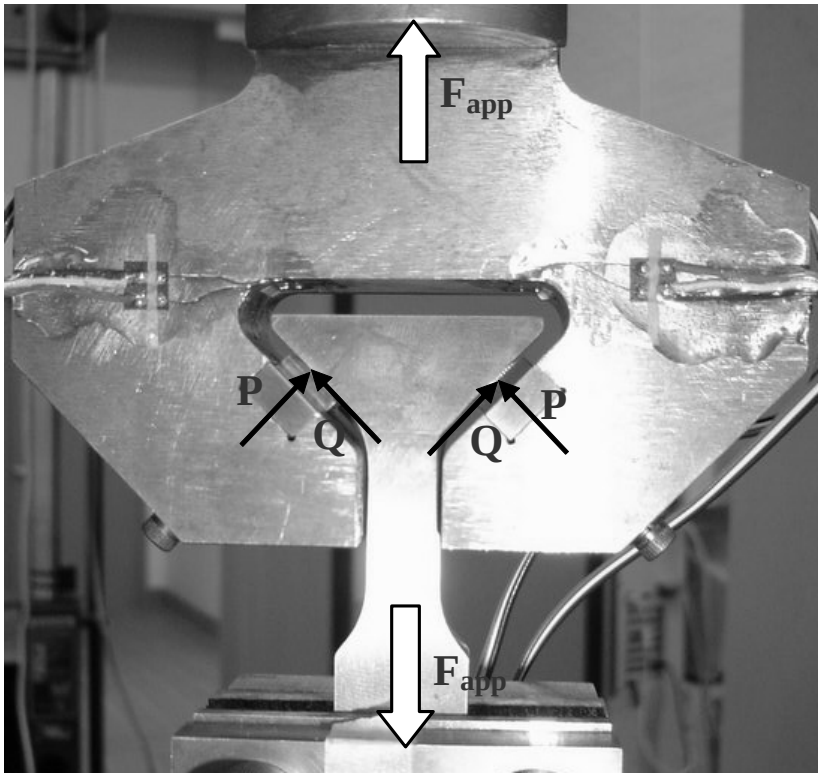


Fig. 3: Photograph of the dovetail fixture, “C”.

### *2.2 Material*

The material used throughout the experiments reported here was Ti-6Al-4V. This material was selected for both the pads and specimens in this study because of its widespread use in aerospace applications and its use in the National Turbine Engine High Cycle Fatigue (HCF) Program within the U.S. Air Force over the past several years. This material was $\alpha+\beta$ forged from mill annealed bar stock then treated at 927°C for 1 hour, fan air cooled, and stress relieved at 704°C for 2 hours. The result of this solution treatment and over aging was a bimodal microstructure with a primary alpha grain size diameter of approximately 20 μm (60% volume fraction) and a balance of lamellar $\alpha+\beta$. This material has a modulus of 116 GPa, and a yield strength of 930 MPa under the ambient laboratory conditions used in the experiments. The microstructure of the material can be seen in Moshier et al. [11].

### *2.3 Experiments and Analysis*

The experimental results for this work have been previously documented [4,6,9]. Conditions (shown in Table 1) were selected from available data to facilitate comparison of the experimental results and analysis that was performed using those conditions. In general, maximum applied bulk stresses between 200 and 300 MPa were selected for stress ratios, $R$, between 0.3 and 0.5. All experiments were performed on specimens of similar dimensions and surface finish without coatings or surface treatments. (Note: the specimen thickness shown for the dovetail specimens corresponds to the distance between the trailing edges of contact on opposite sides of the specimen.) All pads were also of similar surface finish without treatments, and were nominally flat with blending radii of 3 mm, except for one test (B3) featuring cylindrical pads with 50 mm radii. The specimen width was 10 mm for fixtures A and B and 7.6 mm for fixture C. In fixture A, the normal load $P$ applied to the pads was approximately 40 kN,

whereas only 8-9 kN was applied to the pads for Fixture B. In fixture C, only the 45° experimental results are considered in this paper. The clamping loads were coupled to the applied remote load, and ranged between 8.5 and 15.5 kN.

Table 1: Experimental geometries, load conditions, and analysis input parameters.

| Test ID | Max $\sigma_{bulk}$ (MPa) | Bulk R | *Max P (kN) | $Q_{max}$ (kN) | $Q_{min}$ (kN) | Spec. Thickness (mm) | Spec. Width (mm) | Pad Flat Length (mm) | Cycles (times $10^6$) |
|---|---|---|---|---|---|---|---|---|---|
| A1 | 403 | 0.5 | 40.0 | 4.0 | 2.0 | 2 | 10 | 19.05 | 10 |
| A2 | 300 | 0.5 | 39.0 | 3.0 | 1.5 | 2 | 10 | 19.05 | 10 |
| A3 | 299 | 0.5 | 39.4 | 3.0 | 1.5 | 2 | 10 | 6.35 | 10 |
| A4 | 230 | 0.5 | 39.3 | 2.3 | 1.2 | 2 | 10 | 6.35 | 10 |
| B1 | 200 | 0.2 | 9.1 | 1.0 | 0.0 | 4 | 10 | 3.05 | 2 |
| B2 | 300 | 0.4 | 9.0 | 1.3 | 0.7 | 2 | 10 | 3.05 | 2 |
| B3 | 299 | 0.3 | 9.0 | 1.0 | 0.4 | 2 | 10 | 0 | 2 |
| B4 | 230 | 0.2 | 8.0 | 0.8 | 0.1 | 1 | 10 | 3.05 | 5 |
| C1 | 159 | 0.1 | 8.4 (1.8) | 2.8 | -0.6 | 20 | 7.6 | 1.0 | 10 |
| C2 | 296 | 0.4 | 14.1 (9.3) | 1.3 | -1.4 | 20 | 7.6 | 1.0 | 4.49 |
| C3 | 204 | 0.4 | 13.0 (8.3) | 2.4 | -0.5 | 20 | 7.6 | 1.0 | 5.23 |
| C4 | 242 | 0.4 | 15.5 (9.7) | 2.7 | -0.4 | 20 | 7.6 | 1.0 | 5.52 |

* Values in () correspond to minimum values for that parameter.

In fixtures A and B, the tests were performed using a step-loading procedure in which the bulk stress was selected so the specimen can undergo a pre-selected number of cycles without fracturing. Then, the bulk stress was increased by a small percentage, and the block of cycles was repeated. This step process was repeated until specimen fracture, and fatigue limit strength for the selected fatigue life could be interpolated [2]. The step-loading approach was not used for tests in the dovetail fixture (fixture C), but the stress-life (S-N) fatigue lives are similar to the fatigue lives selected for fixtures A and B. The step-loading procedure has been validated for fixtures A and B through comparison of S-N results to the fatigue limit stress data described above [4]. Using the parameter values from each experiment, analyses were performed to allow comparison of local edge of contact (EOC) conditions that produced failure in the number of cycles indicated in Table 1. Each analysis included an evaluation of the axial stress field, via finite element or numerical methods, followed by calculation of the stress intensity factor, *K*, for

an assumed crack growing in the mode I direction. For fixtures A and B, this was a crack that was normal to the applied loading direction. In Fixture C, the mode I crack growth direction was inclined approximately 15° from normal away from the contact area. The resulting stresses were used to assess criteria for crack initiation and the K fields were used to determine the conditions for crack arrest or continued propagation.

The contact stress analysis was conducted on two experiments covering the widest range of behavior from each of the three fixtures, indicated in Table 1. In fixtures B and C, the contact usually undergoes gross slip during early cycles of the test until the coefficient of friction, $\mu$, stabilizes and a transition to partial slip conditions takes place. Thus, the analyses were performed for a cycle in which $\mu$ was stable and partial slip conditions prevailed. Because of questions that arise pertaining to the local coefficient of friction, $\mu$, in the slip region, several values were used for each of the calculations. The analysis assumed a two-dimensional plane strain linear elastic problem for each experiment with quasi-static loading. The surface tractions were calculated for each experiment using singular integral equations with the software CAPRI [12]. The inputs to CAPRI were the pad geometry; the total normal force, $P$; and tangential force, $Q$; bulk stress, $\sigma_{bulk}$; and material properties including Young's modulus, $E$; Poisson's ratio, $\nu$; and coefficient of friction, $\mu$. The subsurface stresses were calculated using Fast Fourier Transform (FFT) techniques that accounted for the effect of specimen thickness on the stress gradient [6].

The surface and subsurface stress fields were then used to correlate with S-N and fracture mechanics models respectively. The surface stress field was used to calculate the equivalent stress, $\sigma_{eq}$, distribution along the contact surface as defined by Murthy et al. [13]. The equivalent stress quantity accounted for the multi-axial stress state and the local stress ratio at each point. It

was then used with a stressed area technique to determine a crack nucleation life, $N_i$, based on data from smooth bar and notched bar fatigue tests [14]. The subsurface stress field below the EOC was used to calculate the mode I stress intensity factor range, $\Delta K$, based on a semi-elliptical surface crack using a weight function approach [15]. An effective stress intensity factor range, denoted $K_{eff}$, was then used as the crack driving force. $K_{eff}$ is dependent on the local stress ratio, $R$, and is defined by Eq. 2 where $m$ is a constant determined empirically from crack growth data [11]. The values of $m$ for this material were 0.72 for $R > 0$ and 0.275 for $R < 0$. Mode mixity was not considered since it has been shown to have negligible effect in these fixtures [3,15].

$$K_{eff} = \Delta K(1-R)^{m-1} \qquad (2)$$

## 3. Results

### *3.1 Shear and Normal Load Histories*

For the three fretting fatigue fixtures discussed here, partial slip conditions prevail during the bulk of the applied cycles, thereby producing the damage of interest. One method for describing and comparing the loading conditions in these experiments, and for comparing the experimental conditions to what occurs in an engine dovetail slot, is to plot the shear force, $Q$, as a function of the normal force, $P$, in the contact region. Such a plot can provide information on the evolution of the stick or slip nature of the region of contact. In fixtures A and B, the normal load $P$ is applied directly while the shear load $Q$ is a direct consequence of applied bulk loads and the compliance of the fixture. In both configurations, $P$ is held constant throughout the experiment. In fixture C, an open hysteresis loop of the $P$ versus $Q$ plot can be seen during the run-in cycles.

In Fig. 4, the conditions for a common laboratory experiment conducted under constant clamping load using either fixture A or B are shown on a plot of $Q$ against $P$. The clamping load

is applied first, represented by line O-A. Two lines bound the region where all combined values of $Q$ and $P$ can take place. The one boundary is when the bodies slide with respect to each other in one direction while the other is when they slide in the other direction. All other points in the enclosed region represent partial slip conditions. The boundaries are given by Eq. 3 where μ is the average coefficient of friction. All sliding must take place along these lines. The lines are denoted as the "slide out line" and the "slide in line" as described by Gean [16] in characterizing the conditions in a dovetail slot in an engine where the blade can tend to slide out of the disk or back into it.

$$Q = \mu P \text{ and } Q = -\mu P \quad (3)$$

In fixture A there is no sliding while fixture B may involve partial slip conditions as the specimen is subjected to cyclic shear loading between points B and C, for example. If the initial shear load produces slip at point B and the coefficient of friction increases, then the slide out line will take on a higher slope and the remainder of the test will be conducted in partial slip. If the conditions are such that slip takes place at one point in the cycle for each cycle, such as in cycling through D-C, then a ratcheting condition will occur. If slip takes place at both maximum and minimum shear load, then the cycle would be represented by D-E. In either of the last two cases, the hysteretic nature of the cycle does not show as a hysteresis loop in a $Q$-$P$ plot such as Fig. 4. Rather, it has to be recognized that once a point in the cycle is reached that touches either of the slide lines in the figure that sliding will take place. The amount of sliding is not reflected in such a plot.

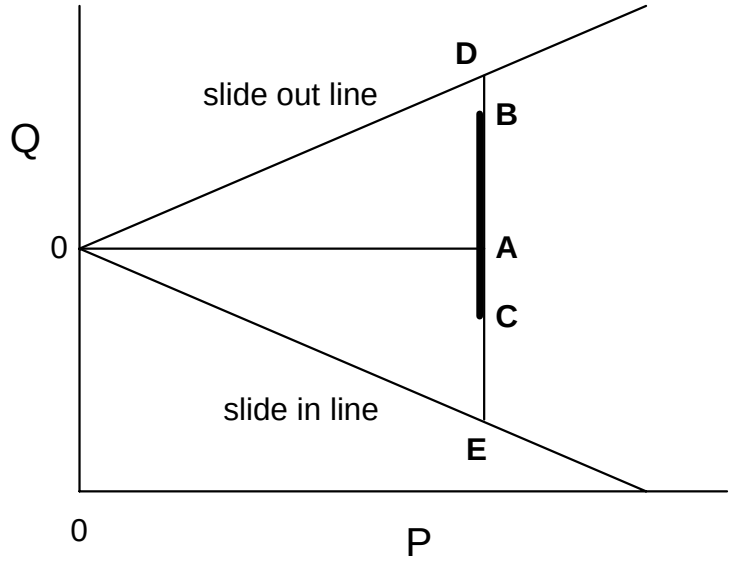


Fig. 4: Plot of *Q* against *P* for any two bodies in contact. Possible paths for simple laboratory experiment with constant *P* are also shown.

The simulated dovetail experimental fixture C produces a condition where the *Q* versus *P* variations are more complicated. The *Q*-*P* path followed during a laboratory experiment is depicted in Fig. 5. Here, the specimen slides along the fixture as load is increased until point A is reached. When the load is decreased, the path from A in the direction of B will be followed. Further cycling with no sliding will then take place along the A-B line, never reaching A or B during the test. Increasing and decreasing load will produce motion as indicated in the Fig. 5. If the load decrease is very large, however, sliding will take place at point B and continue along B-C until minimum load is reached at point C. When the load is increased, the lines C-D (partial slip) and D-A (total slip) will be followed until maximum load is reached at point A. In the dovetail experiment, a complete hysteresis loop A-B-C-D-A can be followed for low values of load ratio, *R*, while for large *R* a path somewhere along the A-B line will be followed.

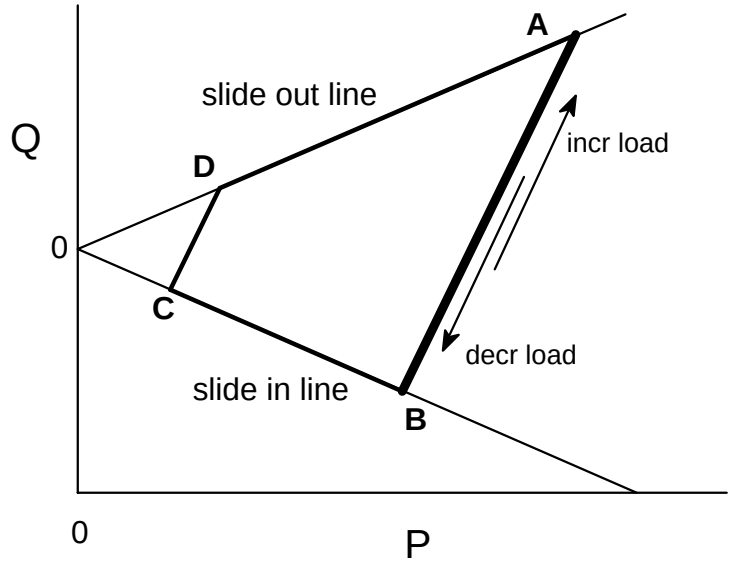

Fig. 5: *Q*-*P* plot for laboratory dovetail fixture C.

For comparison with the laboratory experiments, *Q* versus *P* for a dovetail slot in an engine is shown in Fig. 6. This *Q*-*P* plot for an engine mission indicates the various paths that *Q* and *P* can follow due to changes in engine rpm. Starting at rest with zero applied load, the first increase in engine rpm produces sliding to point A. A decrease in rpm from that point produces a further increase in normal load, *P*, even though the centrifugal load from the blade is decreasing [16]. The reason for this is the expansion of the disk changes with engine rpm (or centrifugal load) so that the net effect is to increase the load *P* with decrease in rpm. If the engine goes through small throttle excursions after the maximum rpm at point A, then the *Q*-*P* path will involve points somewhere along the line A-B with the direction of movement due to increase or decrease in rpm as shown in the figure. If the decrease in rpm is large, the path can go from maximum rpm at A to point B, where "sliding in" starts to take place, to point C where minimum rpm is reached. An increase in rpm from that point will take the path from C to D and then along the line D-A. Complete shut down will follow the path from A to B to the origin. Thus, for small throttle excursions, the behavior will be somewhere along the line A-B while for

large excursions, where low speeds are reached, the path can follow A-B-C-D-A. Note again that unless points A or B are reached during some throttle excursion, the dovetail slot remains in partial slip.

Comparison of the three plots, Figs. 4, 5, and 6 shows that for conditions involving only partial slip the line followed on a *Q*-*P* plot for the constant load experiment, the engine dovetail slot, and the laboratory dovetail specimen has a slope that is zero, negative, or positive, respectively. The laboratory simulations of a fretting fatigue event shown above are seen to be different than what occurs in an engine dovetail, and these differences should be noted when developing models that take load history into account.

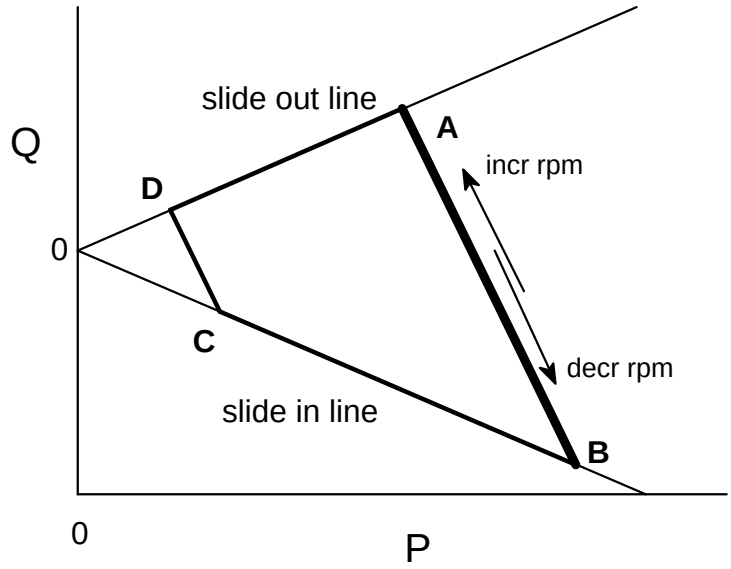


Fig. 6: Q-P plot for an engine dovetail slot.

### *3.2 Bulk Stress*

For the experiments summarized in Table 1, one important quantity of interest that is not featured in the plot of *Q* and *P* is the bulk stress, $\sigma_{bulk}$. In Fig. 7, the conditions used in each fixture are shown in terms of *Q*/*P* as a function of applied bulk stress, $\sigma_{bulk}$. These lines could have been extended by increasing the maximum stress, or by decreasing the stress ratio. In

fixture A (A2 and A3), the position of the $Q/P$ line is constant because $\sigma_{bulk}$ is constrained by $P$. Note that A3 is essentially identical to A2 in the figure. The available $P$ values in this fixture are quite high, allowing the study of conditions that cannot be achieved in fixtures without full load transfer across the contact, but lower $P$ values are limited to those that can restrict gross slip. Changing the specimen thickness may vary the slope of the $Q/P$ lines, but the practical range of thicknesses is limited to between 1 and 4 mm due to hardware and remotely applied load ($\sigma_{bulk}$) constraints.

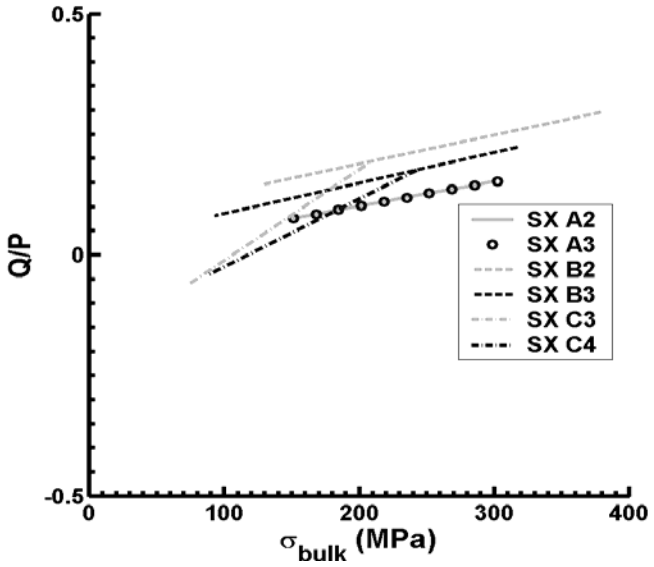


Fig. 7: Range of test conditions for each fixture quantified as the ratio shear, $Q$, to normal, $P$, load versus far field applied bulk stress $\sigma_{bulk}$.

For fixture B, represented in Fig. 7 by lines B2 and B3, the total normal force $P$ can be as low as desired within the ability of the testing hardware to control the load. Also, the total applied bulk stress, $\sigma_{bulk}$, is not constrained by and is not coupled to $P$, allowing the position of the $Q/P$ curves (i.e. the y-intercept) to change. In the experiments shown in Fig. 4, the specimen thickness was nominally the same, but the slope of the $Q/P$ line can be changed by varying the thickness.

In fixture C, $P$ varies in phase with $\sigma_{bulk}$, so it is coupled to but not limited by $P$. The slope of the $Q/P$ versus $\sigma_{bulk}$ curve changes with the value of the remotely applied force. Higher remote loading resulted in a higher $\sigma_{bulk}$, for the same value of $Q/P$. $Q/P$ is dependent on coefficient of friction which is generally independent of load. Also, negative $Q/P$ values can be achieved with the reversal of the shear load during the loading cycle due to initially sliding followed by partial slip conditions during unloading.

In fixtures B and C, a wide variety of pad geometries may be employed. Experiments have been performed using both cylindrical and nominally flat pads with blending radii at the ends of the flat. In fixture A, contact pad geometries are limited to nominally flat pads with relatively large flat lengths, because the remote load is constrained by $P$. The use of very short contact lengths or cylindrical pads in this fixture would not permit full load transfer across the contact without extremely high levels of plastic deformation. In all three fixtures, nominally flat fretting pads may have flat lengths and blending radii varying over a considerable range.

### *3.3 Local Stress Fields*

The tangential component of surface stress, $\sigma_{xx}$, for the three different fixtures under maximum loading is shown in Fig. 8. Here, $x$ is parallel to the surface of the specimen and $a$ is the half contact length. The position values are normalized to allow comparison of the stress fields for different contact lengths. The calculated elastic stress peaks for each case are well above cyclic yield (930 MPa), but only over a very small volume. A sharp stress gradient is shown at the edge of contact in each experiment. The highest peaks occur for fixture C (C3 and C4), while fixtures A and B had slightly lower stress peaks, with the cylindrical pad experiment from fixture B (B3) having the lowest EOC stress peak. The peaks are consistent with the point of crack nucleation for each experiment and decay to far field values within 1 mm of the stress

peak. The stress peaks are also a function of the contact geometry as noted in the legend and summarized in Table 1.

The distribution of $\sigma_{xx}$ below the EOC at maximum load is shown in Fig. 9 as a function of depth below the specimen surface on a semi log plot. The EOC location is also the location of peak $\sigma_{xx}$ at the surface. Here, *y* is the coordinate into the specimen depth. For fixtures A and B, *y* is normal to the surface. For fixture C, *y* is inclined 15° from normal away from the contact area, since this was the crack growth path. For the dovetail experiments (C3 & C4) the subsurface stresses decay the most rapidly and become compressive at a local minimum that occurs at ~100 μm. The local minimums for fixtures A and B are not as well defined. They are tensile and occur closer to the surface than in fixture C, between ~50-100 μm (A2, A3, B2). For the cylindrical pad (B3), the stress field does not decay as rapidly as in the other cases, and the local minimum is not present.

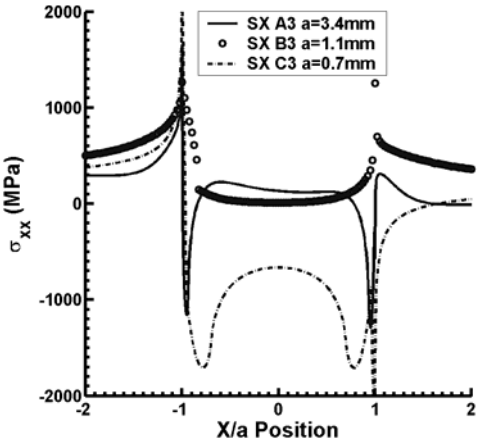


Fig. 8: $\sigma_{xx}$ stress profile along the contact region, where 0.0 corresponds to the center of the fretting pad and negative X values correspond to the trailing EOC.

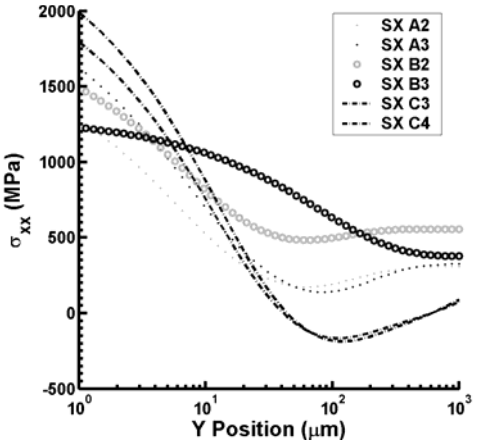


Fig. 9: $\sigma_{xx}$ stress gradient into specimen thickness, from surface at Y=0 to Y=1.0 mm.

### *3.4 Fracture Mechanics Calculations*

Stress intensity factors for cracks along the maximum mode I path were determined from the calculated stress fields using a weight function approach. The effective stress intensity factor

range, denoted by $K_{eff}$, for each experiment as well as the short crack, $K_{th,sc}$, and long crack, $K_{th,lc}$, thresholds for a given crack depth, $a$, are shown in Fig. 10. The short crack threshold was computed using the correction proposed by El Haddad, et. al. [17].

$K_{eff}$ for all three fixtures under nearly all tested conditions falls above $K_{th,sc}$ for cracks below ~100 μm, suggesting that all cracks will propagate to some length, however, not all will propagate to failure. $K_{eff}$ for fixture A is shown to cross the short crack threshold near 10-20 μm crack depths under some loading conditions. The dovetail fixture experiments, however, have a local minimum for $K_{eff}$ at approximately 200 μm where long crack fracture mechanics dominate, indicating a potential for these cracks to arrest. In fixtures A and B, $K_{eff}$ continuously increases and does not have a local minimum.

The most rapidly increasing $K_{eff}$ is shown for fixture B. $K_{eff}$ is similar in magnitude for fixtures A and B for very small flaw sizes, but the rate of increase of $K_{eff}$ for fixture A does not occur until after approximately 100 μm. Crack growth lives, therefore, would be expected to be much longer for experiments using the A fixture than those for the B fixture. If the total lives are similar, then initiation would have taken place earlier in the fixture A experiments than for those in fixture B. The results for the dovetail fixture, on the other hand, show a distinct possibility that initiation could have taken place at stress levels below those that were recorded for total failure. A critical stress level had to be exceeded, according to the $K$ analysis, in order for a crack to not just nucleate, but to exceed the crack growth threshold because of the observed dip in the applied $K$. The difference in the initiation and threshold behavior of fixtures A and B compared to the fixture C can be primarily attributed to the differences in thickness. The finite thickness stress analysis results influence the gradient of $\sigma_{xx}$ into the depth, which also affects $K_{eff}$. For thin specimens it is very difficult to achieve a local minimum in $K_{eff}$.

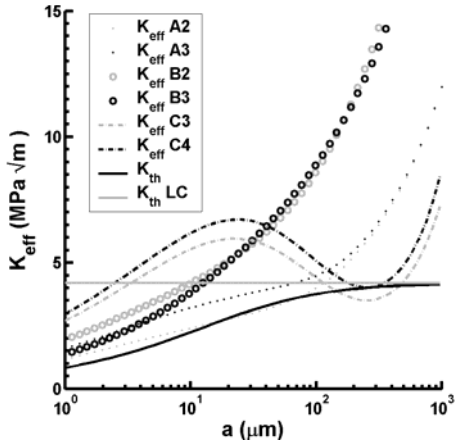


Fig. 7: Effective stress intensity factors calculated for increasing flaw size, *a*.

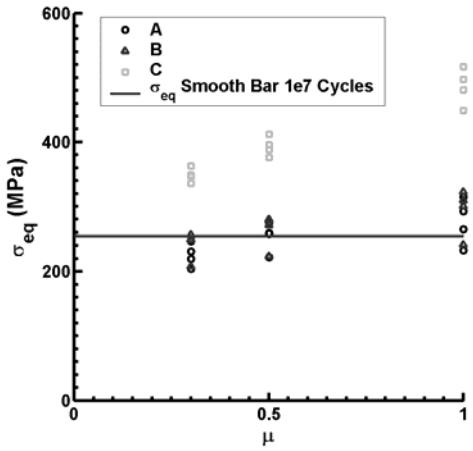


Fig. 8: Equivalent stress as a function of $\mu$ and compared with a smooth bar equivalent stress.

### *3.4 Coefficient of Friction*

The equivalent stress, $\sigma_{eq}$, results for four representative experiments from each fixture are shown in Fig. 8 for varying friction coefficients. The experimental results for fixtures A and B are predicted well by the smooth bar $\sigma_{eq}$ at ten million cycles, however, the equivalent stress results for the dovetail fixtures are shown to be significantly higher than the smooth bar predictions. The assumed value of the coefficient of friction, $\mu$, is also shown to increase $\sigma_{xx}$ more for fixture C than for the other two fixtures. Also, the value of $\sigma_{eq}$ is significantly higher in fixture C. This indicated that cracks might nucleate at a very low fraction of life in the dovetail specimens, which is consistent with the previous fracture mechanics observation that cracks could have nucleated and then arrested. A higher load level was needed to overcome crack arrest. No instrumentation was used to detect the possible initiation that is speculated to have occurred in the dovetail tests. Another consideration is the difference that is speculated to occur in the propagation lives between fixtures A and B based on Fig. 7. One explanation is that fixture B has a shorter crack growth life, but a longer nucleation life than experiments in fixture

A. Fig. 8 however, does not support this conclusion since both fixtures A and B have nominally the same values of the nucleation parameter $\sigma_{eq}$.

**4. Discussion**

A stress-based initiation model predicted the experimental results for fixtures A and B fairly well, as shown in Fig. 8. The initiation model applied to fixture C, however, predicted a much lower life to crack initiation than the actual total lives of the specimens. This may be due to the specimen thicknesses in fixture A and B experiments which were thin (1-2mm) relative to the contact size compared to the fixture C experiments. These results are consistent with other work that has shown that specimens that are thick relative to the contact length, $a$, ($t/a > 5$) produce higher equivalent stress results than the predicted smooth bar results for the same total life [6]. A limitation of the nucleation based tool is that it does not account for the propagation life. The propagation life is expected to be shorter for thin specimens under similar loading, which may account for the difference in the prediction. Also, for the same surface contact conditions, the thin specimens have been shown to have higher subsurface stresses which would also drive higher crack growth rates [6]. Experimental results using interrupted testing for fixture A, however, have shown crack initiation to occur both early and late in life for different test conditions that are both represented in the cases shown here. Therefore, accounting for the propagation life may not fully explain the differences in the initiation based life prediction tool.

Stress intensity factor calculations of $K_{eff}$ versus crack size have been used to predict the minimum crack size that could lead to failure in these experiments. This analysis accounted for the subsurface stress field, which is ignored by the initiation model. The local minimum in the $K_{eff}$ versus $a$ field that often occurs in thick specimens such as the dovetail experiment would predict a crack to grow to a particular length and arrest. This observation explains the short

predicted initiation life compared to the total life in fixture C. Cracks may nucleate very early in life as the model predicts, but fail to grow to fracture or have a very high fraction of life in crack growth. This result is supported from run-out and interrupted experiments that have shown fretting cracks to be present for load cases where failure does not occur. The local minimum in $K_{eff}$ is not predicted for the thin specimens, however, some of these experiments have also been shown to have fretting cracks that did not propagate to failure. This may be due to $K_{eff}$ dropping below the short crack stress intensity factor range, or simply the test was stopped before the crack grew.

The results have also shown that the assumed average friction coefficient, $\mu$, has a significant effect on the stress fields, which has a greater influence on the nucleation life predictions more than the fracture mechanics solutions. The large effect of μ on $N_i$ is because $N_i$ is predicted by the stresses on the contact surface where the effect of $\mu$ is the most pronounced. Although $K_{eff}$ is affected by μ near the surface at the EOC, the effect of $\mu$ on the stress field diminishes 50-100 μm below the surface. It appears from the analysis shown in Fig. 8 that a slip zone coefficient between 0.5 and 1.0 is a reasonable value to assume for the life prediction. This is consistent with experimental and analytical determination of the slip zone coefficient of Ti-6Al-4V on Ti-6Al-4V contact performed by Murthy et al. [13].

The above modeling tools have been shown to be influenced by the loading and contact conditions that were varied in the three fixtures. The crack nucleation criterion depended highly on the surface stress field that is generated by each loading and contact condition. The high normal loads used in Fixture A to prevent gross slip may significantly decrease the run-in process when compared to the other two fixtures. This may result in the local slip zone friction coefficient being different (lower) than that from the other two fixtures because of the lower

amount of relative slip that is seen in the slip zones. The entire bulk load is also transferred to the pad in Fixtures A and C, whereas only a partial load transfer is seen in the Fixture B. The variation in the pad geometry, the frictional behavior, as well as the shear load behavior in the contact region gives rise to a varying shear stress distribution for each fixture. This shear stress distribution on the contact surface has a significant influence on crack-nucleation-based models. Thus, the unique normal and shear loading conditions of each fixture can be used to exercise these initiation-based models.

Various aspects of each fixture also affect the fracture mechanics based models. In this case the subsurface stress field significantly affects the SIF calculations. The applied normal and shear loads influence the magnitude of the subsurface stress distributions. The shape of the subsurface stress field is influenced by the geometry of the contacting pad. It was shown that a large edge radius pad, as was the case for fixture B with the cylindrical pad, produced a stress field that did not decay as rapidly into the subsurface as a smaller edge radius pad that was used in the other two fixtures. The thickness and geometry of the specimen was also shown to influence the subsurface stress field. Fixture C, which had a thicker specimen geometry than the other two fixtures, showed a local minimum occurring in the subsurface stress field. This local minimum was not observed in the other two fixtures with thinner specimens, yet similar pad geometries. The specimen thickness also influenced the predicted propagation life. Therefore, the particular specimen thickness and pad geometry that each fixture is able to use is also an important aspect in exercising the fracture mechanics based models.

## 5. Conclusions

Three different fretting fatigue fixtures are demonstrated to be able to produce a wide range of testing conditions that can be used to further develop current modeling efforts. Both

fracture mechanics and stress-life initiation models were considered for each of the three fretting fatigue fixtures used at the AFRL. Comparisons were made on the same material for long life or runout experiments. It was shown that in fixtures A and B, for the conditions used in these test programs, the fretting fatigue limit correlated well with the stress-life parameter. The use of thin specimens, relative to the contact size, in fixtures A and B along with a higher subsurface stress explain this observation.

For experimental data generated corresponding to similar total lives in the range of $10^6$ to $10^7$ cycles, the stress intensity factor fields were shown to be different for each fixture. The experiments conducted in fixture C appear to have loading conditions where the crack driving force drops below the material crack growth threshold, corrected for small crack behavior, leading to crack arrest. In fixtures A and B, the analysis shows that the crack driving force will generally exceed the small crack corrected threshold for all crack lengths. One loading condition in fixture A was shown to drop slightly below the small crack threshold at a crack depth of approximately 20 μm. It is therefore possible to design loading conditions in these fixtures that nucleate and then arrest cracks. The shapes of the stress intensity factor fields are rather insensitive to changes in the local contact stresses due to changes in the average coefficient of friction.

Based on the experimental conditions covered herein, only the dovetail fixture showed a stress intensity factor field that allowed for cracks to nucleate and arrest until the load required to exceed the long crack growth threshold is surpassed. Thus, the load causing failure in this case relates to the threshold stress intensity factor range and not to a nucleation criterion. On the other hand, fixtures A and B produced stress conditions where the load that produced failure related to a criterion for crack nucleation since any crack that nucleated would continue to

propagate. In general, for any fixture it is important to compute the fracture mechanics driving force, and compare it with the threshold stress intensity factor range including short crack behavior if the data are to be interpreted correctly.

The comparisons among the three fixtures demonstrate that a simple fracture mechanics model is insufficient to explain all of the experimental results. Rather, both crack nucleation and crack propagation appear to be necessary considerations for this total life range of $10^6$ to $10^7$ cycles. Further complicating the matter is the sensitivity of the local stress results to $\mu$, the loading conditions, and the pad and specimen geometries. Each fixture showed the ability to vary these conditions to produce a variety of stress fields in order to exercise these models. The three fixtures can accommodate a variety of specimen thicknesses, fretting pad shapes, contact lengths, and loading conditions. Fixture A is more suited to longer contact lengths while the other two fixtures are able to use shorter flat lengths and cylindrical pad geometries. On the other hand, no gross slip occurs during the run-in process in fixture A, during which the value of $\mu$ may change and wear damage may obscure the presence of other damage mechanisms. Among the three fixtures, a wide variety of conditions involving P, Q, average stresses for the two, and bulk stress can also be accommodated. From these combinations, sufficient data for the development of robust fretting fatigue models can be generated.

**References**


[1] Dobromirski, J.M., "Variables of Fretting Process: Are There 50 of Them?", Standardization of Fretting Fatigue Test Methods and Equipment, STP 1159, M. Helmi Attia, R.B. Waterhouse (eds.), American Society for Testing and Materials, Philadelphia, PA, USA, 60-66 (1992).

[2] Hutson, A.L., Nicholas, T., Olson, S.E., Ashbaugh, N.E., "Effect of Sample Thickness on Local Contact Behavior in a Flat-on-Flat Fretting Apparatus", International Journal of Fatigue, **23**, S445-S453 (2001).

[3] Nicholas, T., Hutson, A.L., John, R., Olson, S., "A Fracture Mechanics Methodology Assessment for Fretting Fatigue," International Journal of Fatigue, **25**, 1069-1077 (2003).

[4] Hutson, A.L., Nicholas, T. Goodman, R., “Fretting Fatigue of Ti-6Al-4V Under Flat-on-Flat Contact”, International Journal of Fatigue, **21**, 663-70 (1999).

[5] Hutson, A.L., Neslen, C., Nicholas, T., "Characterization of Fretting Fatigue Crack Initiation Processes in Ti-6Al-4V," Tribology International, **36**, 2, 133-143 (2003).

[6] Bartha, B.B., Nicholas, T., Farris, T.N., “Modeling of Geometry Effects in Fretting Fatigue,” submitted to Tribology International, June 2004

[7] Hills, D.A., Nowell, D., Mechanics of Fretting Fatigue, 1994, Kluwer Academic Publishers, Dordrecht, The Netherlands.

[8] Golden, P.J., Bartha, B.B., Grandt, A.F., Jr., Nicholas, T., “Measurement of the Fatigue Crack Propagation Threshold of Fretting Induced Cracks in Ti-6Al-4V,” International Journal of Fatigue, **26**, 281-88 (2004).

[9] Moshier, M.A., Nicholas, T., Hillberry, B., “Load History Effects on Fatigue Crack Growth Threshold for Ti-6Al-4V and Ti-17 Titanium Alloys,” International Journal of Fatigue, **23**, S253-58 (2001).

[10] Golden, P.J., Nicholas, T., “The Effect of Angle on Dovetail Fretting Experiments in Ti-6Al-4V,” Fatigue and Fracture of Engineering Materials and Structures, **28**, 1169-75 (2005).

[11] B.P. Conner, B.P., T. Nicholas, T., “Using a Dovetail Fixture to Study Fretting Fatigue and Fretting Palliatives,” ASME Journal of Engineering Materials and Technology, in press.

[12] Murthy, H., Harish, G., Farris, T.N., “Efficient Modeling of Fretting of Blade/Disk Contacts Including Load History Effects,” Journal of Tribology, **126**, 56-64 (2004).

[13] Murthy, H., Rajeev, P.T., Farris, T.N., D.C. Slavik, D.C., “Fretting Fatigue of Ti-6Al-4V Subjected to Blade/Disk Contact Loading,” Proceedings of Developments in Fracture Mechanics for the New Century, 50th Anniversary of Japan Soc of Materials Science, 41-48 (2001).

[14] Slavik, D.C., McClain, R.D., Farris, T.N., Murthy, H., “Fatigue Crack Initiation Modeling for Application with Stress Gradients in Smooth and Notched Geometries,” Proceedings of the 6$^{th}$ Annual High Cycle Fatigue Conference, Jacksonville, FL, (2001).

[15] Golden, P.J., A.F. Grandt, A.F., Jr., “Fracture mechanics based fretting fatigue life predictions in Ti–6Al–4V,” Engineering Fracture Mechanics, **71**, 2229-43 (2004).

[16] Gean, M.C., "Finite Element Analysis of the Mechanics of Blade Disk Contacts," M.S. Thesis, School of Aeronautics and Astronautics, Purdue University, West Lafayette, IN, (2004).

[17] El Haddad, M.H., Smith, K.N., Topper, T.H., “Fatigue Crack Propagation of Short Cracks,” ASME Journal of Engineering Materials and Technology, **101**, 42-46 (1979).